nanomaterials

MDPI

Article

Synergistic Effect of Y Doping and Reduction of TiO_2 on the Improvement of Photocatalytic Performance

Xijuan Li [1], Hongjuan Zheng [2,*], Yulong Wang [3], Xia Li [1,2], Jinsong Liu [1], Kang Yan [2], Jing Wang [2] and Kongjun Zhu [2,*]

[1] College of Materials Science and Technology, Nanjing University of Aeronautics and Astronautics, Nanjing 210016, China; lxjnuaa@163.com (X.L.); lixia170904@nuaa.edu.cn (X.L.); jsliu@nuaa.edu.cn (J.L.)
[2] State Key Laboratory of Mechanics and Control for Aerospace Structures, Nanjing University of Aeronautics and Astronautics, Nanjing 210016, China; yankang@nuaa.edu.cn (K.Y.); wang-jing@nuaa.edu.cn (J.W.)
[3] Department of Applied Physics, The Hong Kong Polytechnic University, Hong Kong 999077, China; yulong1.wang@polyu.edu.hk
* Correspondence: zhenghj2012@126.com (H.Z.); kjzhu@nuaa.edu.cn (K.Z.)

Abstract: Pure TiO_2 and 3% Y-doped TiO_2 (3% Y-TiO_2) were prepared by a one-step hydrothermal method. Reduced TiO_2 (TiO_2-H_2) and 3% Y-TiO_2 (3% Y-TiO_2-H_2) were obtained through the thermal conversion treatment of Ar-H_2 atmosphere at 500 °C for 3 h. By systematically comparing the crystalline phase, structure, morphological features, and photocatalytic properties of 3% Y-TiO_2-H_2 with pure TiO_2, 3% Y-TiO_2, and TiO_2-H_2, the synergistic effect of Y doping and reduction of TiO_2 was obtained. All samples show the single anatase phase, and no diffraction peak shift is observed. Compared with single-doped TiO_2 and single-reduced TiO_2, 3% Y-TiO_2-H_2 exhibits the best photocatalytic performance for the degradation of RhB, which can be totally degraded in 20 min. The improvement of photocatalytic performance was attributed to the synergistic effect of Y doping and reduction treatment. Y doping broadened the range of light absorption and reduced the charge recombination rates, and the reduction treatment caused TiO_2 to be enveloped by disordered shells. The remarkable feature of reduced TiO_2 by H_2 is its disordered shell filled with a limited amount of oxygen vacancies (O_Vs) or Ti^{3+}, which significantly reduces the E_g of TiO_2 and remarkably increases the absorption of visible light. The synergistic effect of Y doping, Ti^{3+} species, and O_Vs play an important role in the improvement of photocatalytic performances. The discovery of this work provides a new perspective for the improvement of other photocatalysts by combining doping and reduction to modify traditional photocatalytic materials and further improve their performance.

Keywords: photocatalysis; TiO_2; Y doping; H_2 reduction; hydrothermal method

Citation: Li, X.; Zheng, H.; Wang, Y.; Li, X.; Liu, J.; Yan, K.; Wang, J.; Zhu, K. Synergistic Effect of Y Doping and Reduction of TiO_2 on the Improvement of Photocatalytic Performance. *Nanomaterials* **2023**, *13*, 2266. https://doi.org/10.3390/nano13152266

Academic Editor: Barbara Bonelli

Received: 6 July 2023
Revised: 31 July 2023
Accepted: 1 August 2023
Published: 7 August 2023

1. Introduction

Among the various semiconductors, titanium dioxide (TiO_2) is considered a useful photocatalyst for the treatment of water pollution and water splitting, owing to its minimal toxicity, strong oxidation capacity, and ready availability [1–6]. In recent decades, many research articles have reported the performance, synthesis methods, as well as the reaction mechanisms of TiO_2 in photocatalytic systems [7–9]. The crystalline phase of TiO_2 remarkably affects its photocatalytic activity. Rutile, anatase, and brookite are the three main crystalline phases of TiO_2 [10]. The photocatalytic performance of pure anatase TiO_2 is better than that of rutile, whereas the brookite phase is unstable and does not show appreciable photoactivity [11]. However, the wide bandgap (E_g; anatase, ~3.20 eV) limits light absorption to the UV region of the solar spectrum (~4% of the total solar irradiance), thus affecting photocatalytic activity [12]. Moreover, the high recombination of the photogenerated electron–hole (e^-–h^+) pair has been proven to reduce photocatalytic efficiency [13]. Many approaches, including metal (Al^{3+}, Zn^{2+}, Fe^{3+}, Ce^{3+}, Mn^{2+}, Ag^+) [14–16] and nonmetal doping [17], the deposition of noble metal (Au, Pt) [18,19], and construction

of heterojunctions with other semiconductors [20,21], have been explored to overcome these limitations.

Among these methods, rare earth (RE) metal doping is a popular technique to reduce the recombination rate of photogenerated carriers and shift the absorption wavelength to the visible region and increase the photoactivity of TiO_2 [22,23]. Furthermore, RE metal doping shows other benefits, such as the ability to concentrate pollutants at the TiO_2 photocatalyst surface, inhibit the phase transformation from anatase to rutile, and decrease the crystallite size [24,25]. Many studies reported that the concentration of RE metal dopant affects the photoactivity, with the optimum achieved at concentrations below 5 wt.% [25]. Among all the RE ions, yttrium (Y) ion is considered a typical dopant used to modify the electronic structure and optical properties of TiO_2 [26]. Specifically, it has been found that the Y-doped TiO_2 can reduce the recombination rate of photogenerated electrons/holes pairs, which improves the photocatalytic efficiency of TiO_2 [27]. The effect of Y-doped TiO_2 on photocatalytic activity has been recently reported in several studies [28,29].

In addition to RE metal doping, reduced TiO_2, which is obtained by high-temperature treatments in various reducing atmospheres (e.g., vacuum, Ar, Ar-H_2, and pure H_2) [30–32] or thermite reduction [33], reduction with sodium borohydride [34], and Ti^{3+} self-doping [35,36], has shown tremendous potential as a photocatalyst in wastewater treatment and water splitting recently. The enhanced photocatalytic performance of reduced TiO_2 is related to a significant decrease in E_g and increased light absorption due to the introduction of oxygen vacancies (O_V) or the formation of Ti^{3+} centers in the TiO_2 lattice [34]. Current studies on reduced TiO_2 focused on the relationship between the Ti^{3+} or O_V concentration and photocatalytic activity of TiO_2 and comparison of the reduction degree caused by different reduction methods. However, the synergistic effect of RE doping and reduction treatment for TiO_2 photocatalysts has not been reported yet.

In this work, pure anatase TiO_2, Y-doped TiO_2, and their respective reduced products were prepared to verify the synergistic effect of Y doping and reduction treatment for TiO_2 photocatalysts. Pure anatase TiO_2 and Y-doped TiO_2 were obtained by a one-step hydrothermal method, reduced TiO_2 and reduced Y-doped TiO_2 were formed by heat treatment in an Ar-H_2 atmosphere at 500 °C for 3 h. The crystalline phase, morphological features, and photocatalytic properties of four types of TiO_2 were compared systematically. By comparing TiO_2 and Y-doped TiO_2, the effect of RE doping on the improvement of photocatalytic performance could be obtained. Similarly, by comparing TiO_2 with reduced TiO_2, the effect of reduction treatment by H_2 on the improvement of photocatalytic performance can be obtained. By comparing TiO_2, which are simultaneously doped and reduced, with pure TiO_2, Y-doped TiO_2, and reduced TiO_2, it can be verified the existence of a coupling effect of RE doping and reduction treatment on the improvement of photocatalytic performance. Ultimately, a positive effect of the combination of Y doping and reduction of TiO_2 on the improvement of photodegradation activity of organic pollutants under simulated sunlight irradiation was found, and their possible photocatalytic mechanism was proposed. The aim of this study was to develop an understanding of the synergistic effect of Y doping and reduction of TiO_2 on the improvement of photocatalytic performance.

2. Experimental

2.1. Materials

Titanium isopropoxide (TIP), $Y(NO_3)_3 \cdot 6H_2O$, absolute ethanol, acetic acid, and nitric acid (HNO_3) were received from Sinopharm Chemical Reagent Co., Ltd., Shanghai, China. All chemicals were not further purified during use.

2.2. Preparation of Pure TiO_2 and Y-Doped TiO_2 Nanoparticles

A total of 4.2 mL of TIP, 16.8 mL of absolute ethanol, and 1.68 mL of acetic acid were mixed under continuous stirring to form solution A. Solution B was composed of a certain amount of $Y(NO_3)_3 \cdot 6H_2O$ dissolved in 21 mL of deionized water with a pH value adjusted to 2.5 by dilute HNO_3 (1 mol·L^{-1}). The molar ratio of Y/Ti in solution B was set to 0, 1%,

2%, 3%, 4%, and 5%, respectively. Then, solution B was added into solution A to obtain Y-doped TiO_2 sol. After stirring for 30 min, the Y-doped TiO_2 sol was transferred into a 70 mL Teflon vessel. The Teflon vessel was placed into stainless-steel autoclaves. Then, the autoclaves were put in an oven and heated to 180 °C for 12 h. Then, the autoclaves were cooled to room temperature after hydrothermal treatment. The final products were filtered, washed, and dried at 80 °C for 12 h.

2.3. Preparation of Reduced TiO_2 and Y-Doped TiO_2 Nanoparticles

TiO_2 and Y-doped TiO_2 nanoparticles were placed in a tube furnace, respectively, and then evacuated to a base pressure of about 0.5 Pa. The tube was filled with Ar-H_2 (95 vol %–5 vol %) atmosphere to normal pressure. The samples were heated at 500 °C with a heating rate of 5 °C /min for 3 h in Ar-H_2 flow to obtain the final reduced pure TiO_2 and Y-doped TiO_2 products by H_2.

2.4. Photocatalytic Test

The photocatalytic activity test was conducted using RhB as a simulated pollutant and a 300 W Xe lamp as a simulated sunlight source (PLS-SXE300/300UV, Trusttech Co., Ltd., Beijing, China) to irradiate the pollutant. In a typical photocatalytic process, 10 mg of the catalyst was dispersed into 100 mL of the RhB solution (10 mg L^{-1}) in a 200 mL double-layer reactor cooled by running water to maintain a temperature of 25 °C, and the mixture was magnetically stirred with 300 rpm in the dark for 1 h to achieve an adsorption–desorption balance. Then, the xenon lamp was turned on, and 5 mL of the suspension was collected at every 10 min interval and centrifuged (9000 rpm, 5 min) to remove the catalyst powders. The total irradiation time of all samples was 1 h. The degradation rate of RhB was calculated by converting the absorbance into concentration using the dye standard curve by a UV–vis spectrophotometer.

2.5. Characterization

The phase structure of the products was determined using X-ray diffraction (XRD) (Bruker D8Advance diffractometer) with Cu K_α radiation (λ = 1.5418 Å). The structural information of products was obtained using high-resolution transmission electron microscopy (HRTEM) by a JEM-2100F at 200 kV. X-ray photoelectron spectroscopy (XPS) measurements were carried out using the AXIS-Ultra DLD system. The UV–vis diffuse reflectance absorption spectra (DRS) of samples were used to determine the bandgap by the PE Lambda 950 spectrometer with $BaSO_4$ as reference. The Brunauer–Emmett–Teller (BET) method with a JW-BK200B was used to evaluate the specific surface area of the products.

3. Results and Discussion

3.1. Structure and Morphology Characterization

Pure TiO_2 and various Y-doped TiO_2 (1–5%) were prepared in advance to verify their phase composition and photocatalytic performance for the degradation of RhB. XRD was used to characterize and compare the crystalline phase of samples. All samples show the single anatase phase (Figure S1a). The catalytic activities were evaluated by the degradation of RhB under simulated sunlight irradiation and the maximum photocatalytic performance for the degradation of RhB when the Y dopant concentration was 3% (Figure S1b). Therefore, 3% Y-doped TiO_2 was selected as a typical research object for rare earth doping. Figure 1 shows the crystalline phase of pure TiO_2, 3% Y-doped TiO_2 (3% Y-TiO_2), reduced TiO_2 by H_2 (TiO_2-H_2), and reduced 3% Y-doped TiO_2 (3% Y-TiO_2-H_2). All four samples have significant diffraction peaks representing the characteristic of a single anatase phase (PDF No. 211272). Anatase is the only crystalline phase present in the structure of TiO_2-H_2 and 3% Y-TiO_2-H_2, indicating that no phase transformation occurs in the annealing process of H_2 reduction at 500 °C. After annealing, the colors of TiO_2-H_2 and 3% Y-TiO_2-H_2 change from white to gray black. The refraction of Y_2O_3 is not observed in the XRD patterns of 3% Y-TiO_2 or 3% Y-TiO_2-H_2, indicating that the content of Y_2O_3 is below the detection

limit. No diffraction peak shift is observed for all Y-modified samples, demonstrating that Y^{3+} species exists at the crystal boundary or surface rather than in the inner crystalline structure of TiO_2. The increased diffraction peak intensities of TiO_2-H_2 and 3% Y-TiO_2-H_2 after annealing indicate the increased crystallinity of samples in comparison with those of pure TiO_2 and 3% Y-TiO_2.

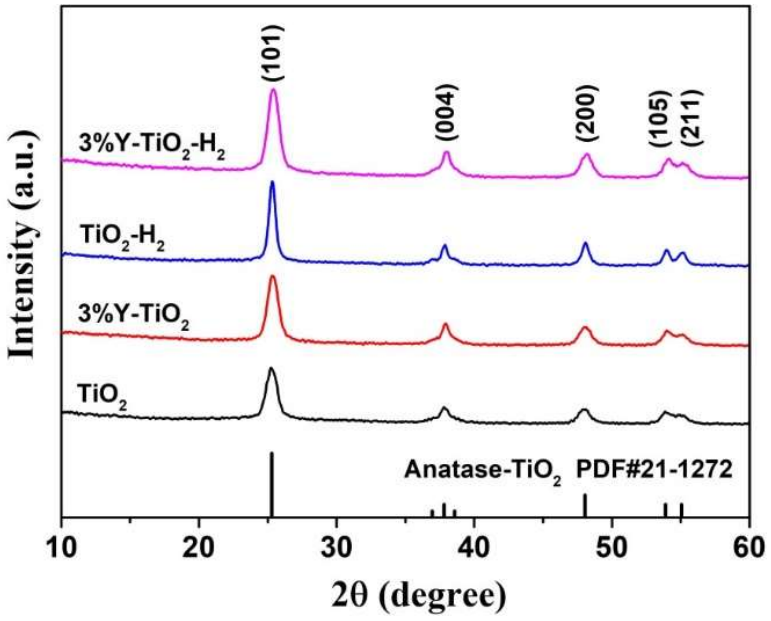

Figure 1. XRD patterns of pure TiO_2, 3% Y-TiO_2, TiO_2-H_2, and 3% Y-TiO_2-H_2 samples.

The morphology and structure of all four samples are investigated by HRTEM. The low-magnification TEM images and statistical particle size distribution of TiO_2, 3% Y-TiO_2, TiO_2-H_2, and 3% Y-TiO_2-H_2 are shown in Figure 2a–d and their insert, respectively. All samples are primarily composed of dispersed circular, rectangular, and some irregular-shaped nanoparticles with average sizes ranging from 8 nm to 11 nm. The grain sizes of TiO_2-H_2 and 3% Y-TiO_2-H_2 increase slightly but not significantly after annealing. High-magnification TEM images show clear lattice fringes, which is indicative of the high crystallinity of TiO_2 and 3% Y-TiO_2 (Figure 2e,f). However, high-magnification TEM images of TiO_2-H_2 and 3% Y-TiO_2-H_2 illustrate a core–shell structure with a ~1.5 nm-thick disordered surface shell (Figure 2g,h), which is not observed on the surfaces of TiO_2 and 3% Y-TiO_2 prepared by the single hydrothermal method. Four samples have lattice spacings of 0.34 nm in the same way as in Figure 2e, which is consistent with its (101) planes (Figure 2e–h). The elemental mapping images of 3% Y-TiO_2-H_2 with individual elements of Ti, O, and Y are shown in Figure 2i. Ti, O, and Y are uniformly distributed throughout the particle space, proving the presence of Y elements in Y-doped TiO_2 samples.

The surface areas of all products were estimated by the BET analysis; their N_2 adsorption–desorption isotherms are shown in Figure 3. The specific surface areas of pure TiO_2 and 3% Y-TiO_2 are 148.58 (Figure 3a) and 160.17 m^2/g (Figure 3b), respectively, which can be related to changes in the morphology of the TiO_2 after doping with Y. Based on the XRD results, no diffraction peak shift is observed for 3% Y-doped TiO_2, demonstrating that the Y^{3+} species exists at the crystal boundary or surface rather than in the inner crystalline structure of TiO_2. Therefore, it is speculated that the adhesion of Y^{3+} species to the surface of particles increases the roughness of the particle surface, resulting in an increase in the specific surface area. The specific surface areas of TiO_2-H_2 and 3% Y-TiO_2-H_2 are 85.94 (Figure 3c) and 117.42 m^2/g (Figure 3d), respectively, which is lower compared to pure TiO_2 and 3% Y-TiO_2. This may be attributed to the grain growth and slight aggregation caused by high-temperature annealing treatment, which is consistent with the results of the statistical particle size distribution in TEM images.

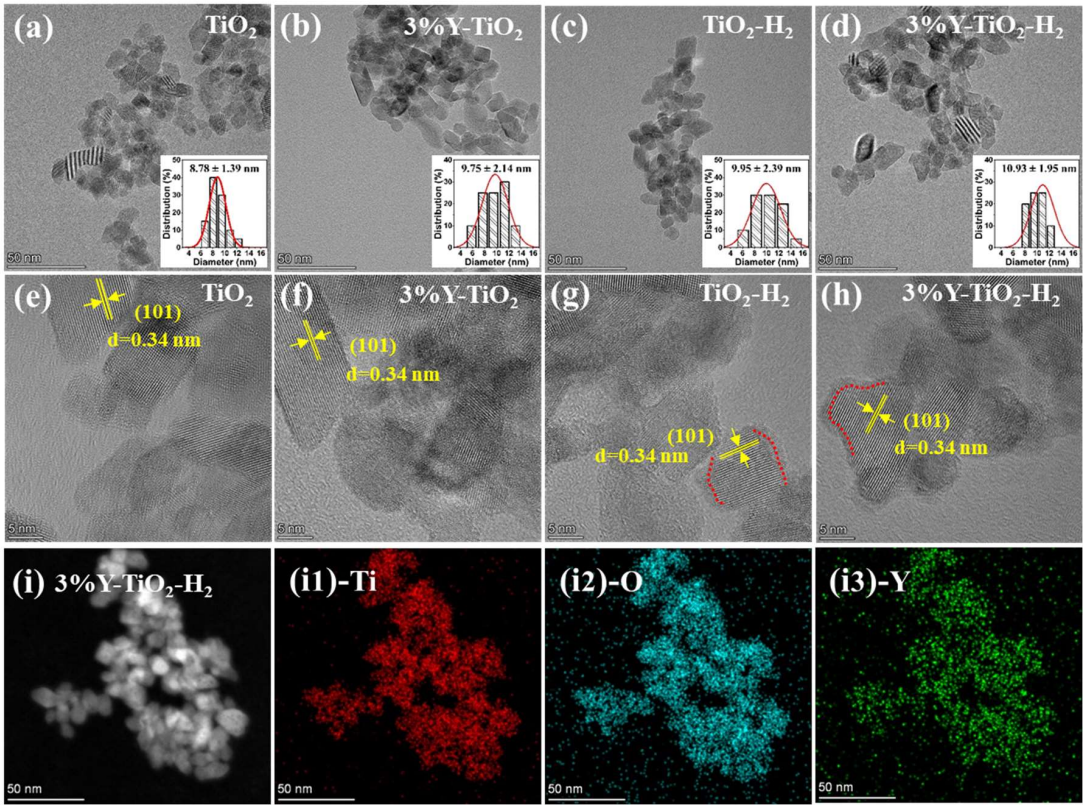

Figure 2. HRTEM images of (**a**,**e**) TiO_2, (**b**,**f**) 3% Y-TiO_2, (**c**,**g**) TiO_2-H_2, and (**d**,**h**) 3% Y-TiO_2-H_2 (inset is the corresponding statistical particle size distribution). (**i**) Elemental mapping of 3% Y-TiO_2-H_2 for Ti (**i1**), O (**i2**), and Y (**i3**).

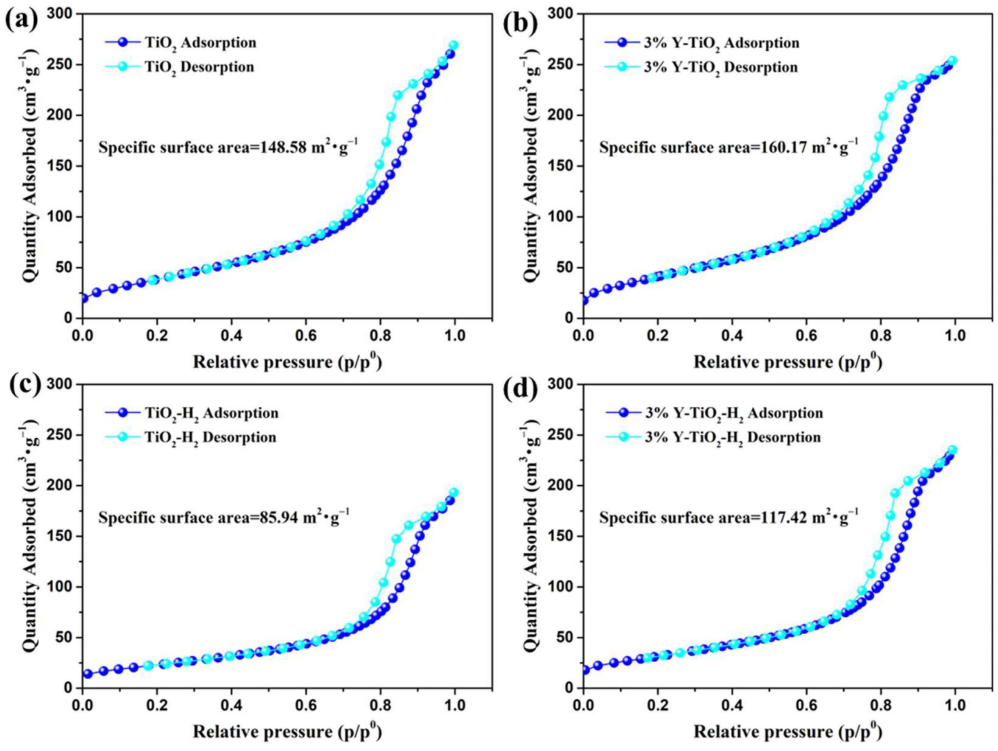

Figure 3. N_2 adsorption–desorption isotherms of TiO_2 (**a**), 3% Y-TiO_2 (**b**), TiO_2-H_2 (**c**), and 3% Y-TiO_2-H_2 (**d**).

Based on the survey scanning the XPS spectra of four samples, all labeled peaks were attributed to Ti 2p and O 1s (Figure S2). Furthermore, a weak Y 3d peak is observed at ~158 eV, indicating the presence of Y^{3+} species on the surface of 3% Y-TiO_2 and 3% Y-TiO_2-H_2 samples. The high-resolution XPS spectra of Ti 2p for four samples are shown in Figure 4a–d. TiO_2 and 3% Y-TiO_2 exhibit two peaks at 458.4 and 464.2 eV, which are attributed to 2p3/2 and 2p1/2 of Ti^{4+}, respectively [37]. For TiO_2-H_2 and 3% Y-TiO_2-H_2, these peaks shift to low values, broaden, and become unsymmetrical compared with those of pure TiO_2 and 3% Y-TiO_2, indicating a different bonding environment (Figure S3) [38]. The fitting curves show that the two peaks of Ti 2p are divided into four peaks, found at 458.3 and 464.0 eV, respectively, corresponding to the 2p3/2 and 2p1/2 peaks of Ti^{4+}, and at 457.8 and 463.2 eV, respectively, corresponding to the 2p3/2 and 2p1/2 peaks of Ti^{3+} [39]. The Ti^{3+} state indicates that TiO_2-H_2 and 3% Y-TiO_2-H_2 are partially reduced through H_2 reduction.

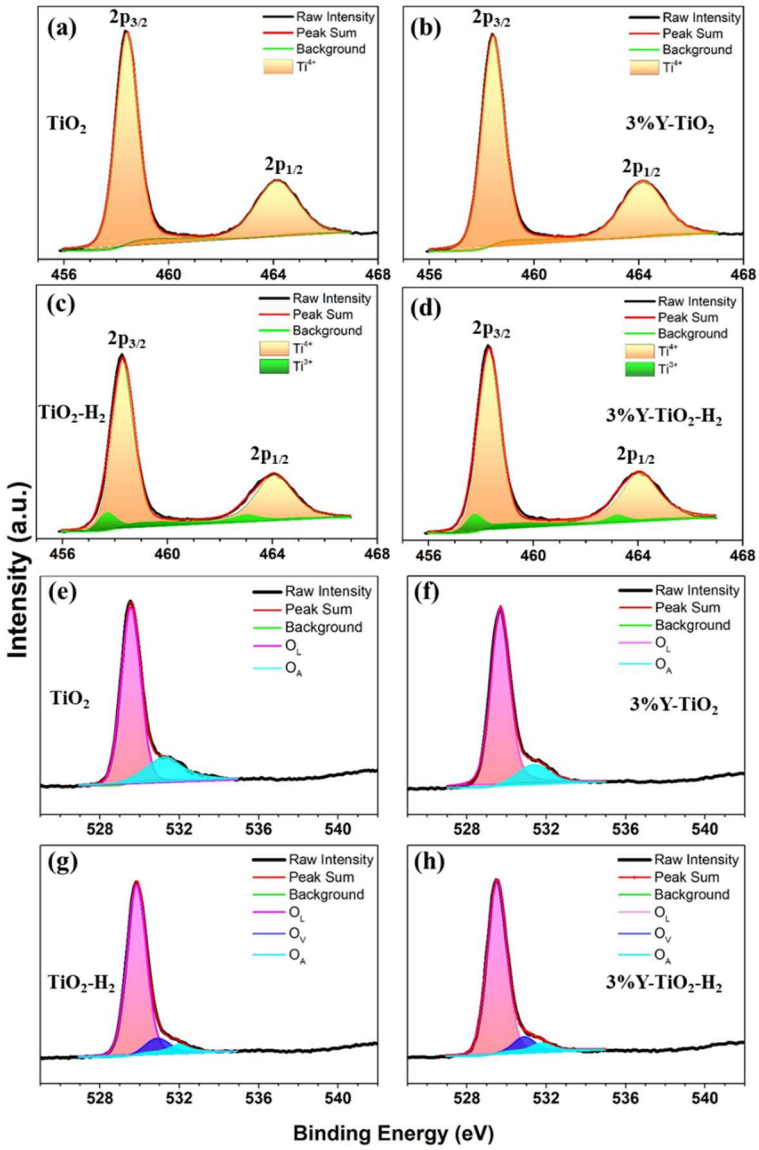

Figure 4. XPS spectra for Ti 2p of TiO_2 (**a**), 3% Y-TiO_2 (**b**), TiO_2-H_2 (**c**), 3% Y-TiO_2-H_2 (**d**), and for O 1s of TiO_2 (**e**), 3% Y-TiO_2 (**f**), TiO_2-H_2 (**g**), 3% Y-TiO_2-H_2 (**h**).

The high-resolution XPS spectra of O 1s for four samples are shown in Figure 4e–h. In TiO_2 and 3% Y-TiO_2, two nonsymmetric fitted peaks signify the presence of two O species. The binding energy at 529.6 eV is ascribed to the characteristic peak of Ti-O in anatase

TiO_2, namely, lattice oxygen (O_L). The binding energy at 531.4 eV is attributed to the O-H, i.e., adsorbed oxygen (O_A) [40]. In TiO_2-H_2 and 3% Y-TiO_2-H_2, three nonsymmetric fitted peaks are obtained. Except O_L (529.8 eV) and O_A (531.9 eV), the small peak centered at around 530.9 eV can be assigned to O_Vs [41]. The estimated ratio of O_V to O_L (O_V/O_L) of TiO_2-H_2 is 0.09 according to the calculated integral areas of the corresponding peaks. For 3% Y-TiO_2-H_2, the ratio of O_V/O_L decreases to 0.07, indicating that the Y^{3+} on the surface or grain boundary of TiO_2 by Y doping may slightly inhibit the formation of O_Vs. Furthermore, the content of O_A decreases sharply for TiO_2-H_2 and 3% Y-TiO_2-H_2, implying that -OH groups or adsorbed water on the surface of TiO_2-H_2 and 3% Y-TiO_2-H_2 are largely scavenged during annealing.

Figure 5a shows the UV–vis DRS of four samples. The light absorption edge of pure TiO_2 is approximately 390 nm. The light absorption edges of 3% Y-TiO_2, TiO_2-H_2, and 3% Y-TiO_2-H_2 gradually blue-shift compared with that of TiO_2, and the light absorption capacities in their visible region are gradually enhanced. The light absorption in the region from ~400 nm to the near-infrared region is significant in TiO_2-H_2 and higher in 3% Y-TiO_2-H_2.

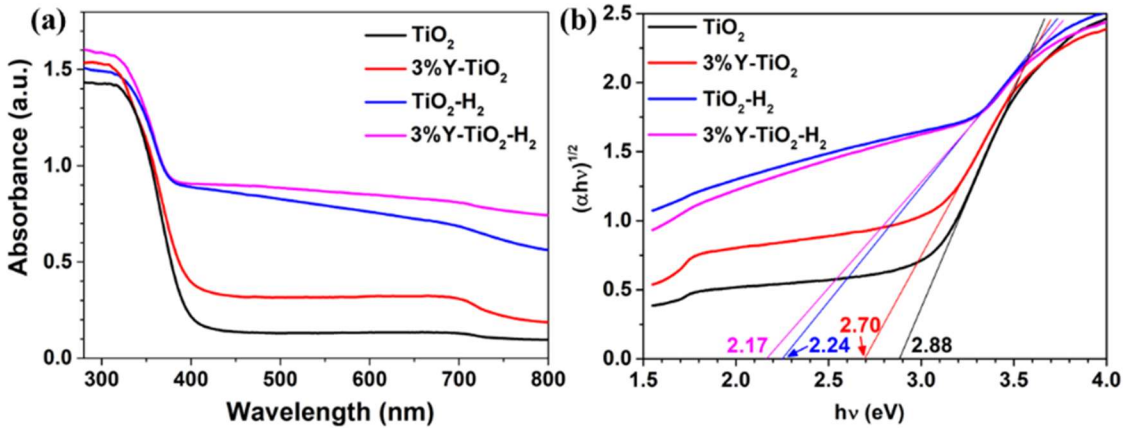

Figure 5. (**a**) UV–vis diffuse reflectance absorption spectra and (**b**) corresponding bandgap of TiO_2, 3% Y-TiO_2, TiO_2-H_2, and 3% Y-TiO_2-H_2 samples.

The E_g can be calculated in accordance with the formula:

$$(\alpha h\upsilon)^{1/n} = A(h\upsilon - E_g), \quad (1)$$

Among them, α, h, ν, and A are the absorption coefficient, Planck's constant, frequency of the incident light, and a constant, respectively. For direct and indirect transition semiconductors, n is 1/2 and 2, respectively. The value of n is 2 for the anatate TiO_2. In Figure 5b, the E_g values of TiO_2, 3% Y-TiO_2, TiO_2-H_2, and 3% Y-TiO_2-H_2 obtained from the tangent intercept are 2.88, 2.70, 2.24, and 2.17 eV, respectively.

3.2. Photocatalytic Test

The effect on the catalytic activities of all four samples is evaluated by the degradation of RhB under simulated sunlight irradiation, as shown in Figure 6. The UV–vis absorption spectra of TiO_2, 3% Y-TiO_2, TiO_2-H_2, 3% Y-TiO_2-H_2 are separately displayed in Figure 6a–d, and the degradation efficiency curves are summarized in Figure 6e. For pure TiO_2, RhB can be totally degraded in approximately 60 min, whereas RhB can be totally degraded by 3% Y-TiO_2 in 40 min, which is shorter than that by pure TiO_2. This result indicates that a proper amount of RE doping has a positive effect on photocatalytic performance. For TiO_2-H_2, RhB can be totally degraded only in 30 min, which is beneficial for the reduction role of TiO_2. Interestingly, RhB can be totally degraded by 3% Y-TiO_2-H_2 in 20 min, which is less time than those of other samples. The combined action of 3% Y doping and reduction

by H_2 is beneficial to the photodegradation activity of TiO_2, and the co-modified catalyst exhibits higher photocatalytic activity than any single-modified catalyst.

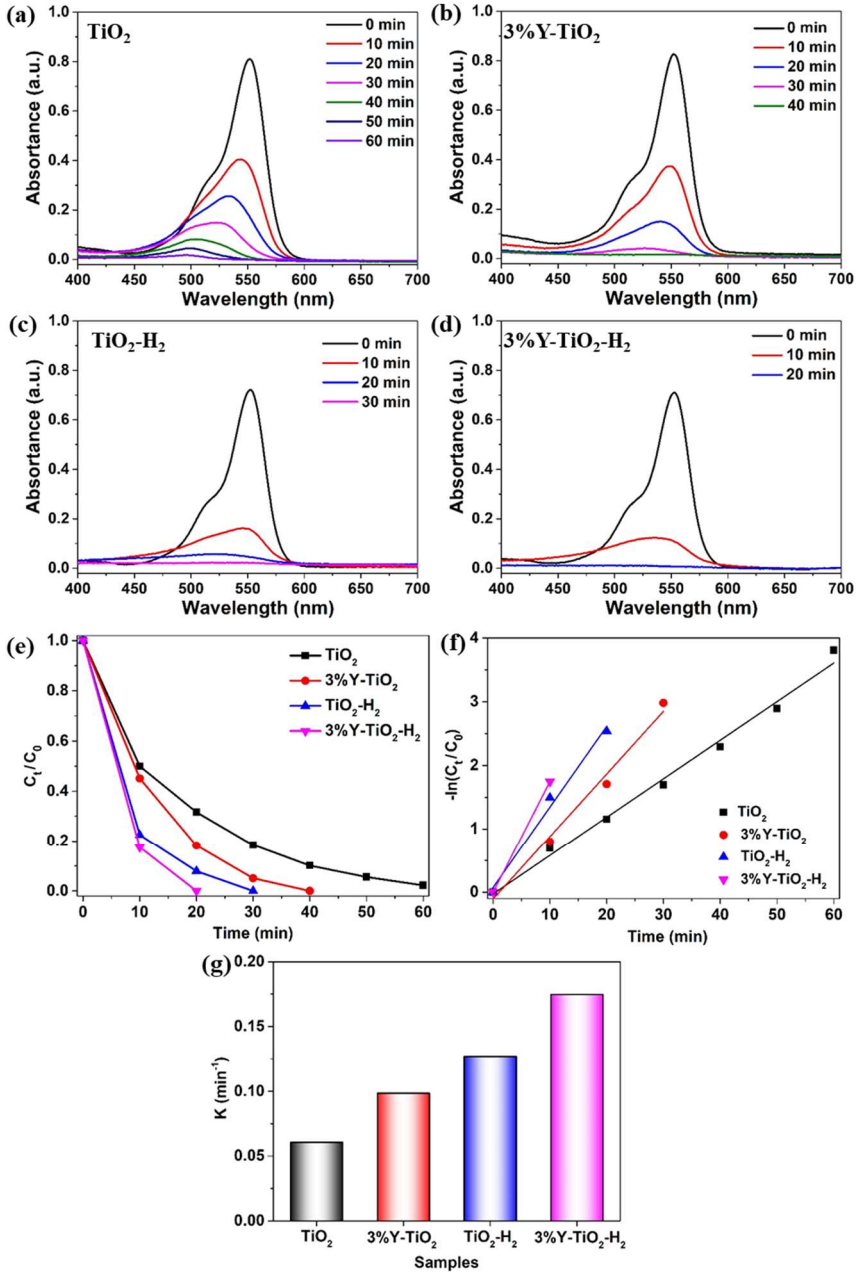

Figure 6. UV–vis absorption spectra of TiO_2 (**a**), 3% Y-TiO_2 (**b**), TiO_2-H_2 (**c**), 3% Y-TiO_2-H_2 (**d**), degradation efficiency curves (**e**), kinetic curves (**f**), and reaction rate constant (**g**).

The kinetics of the photocatalytic activities of all four samples follow the first-order reaction:

$$-\ln(C_t/C_0) = k_1 t, \quad (2)$$

where k_1 is the pseudo-first-order reaction rate constant (min^{-1}) obtained from the slope of $-\ln(C_t/C_0)$ vs. t, as shown in Figure 6f,g. The k_1 values of TiO_2, 3% Y-TiO_2, TiO_2-H_2, and 3% Y-TiO_2-H_2 are 0.0606, 0.0985, 0.1269, and 0.1746, respectively, indicating the efficient photodegradation activity of 3% Y-TiO_2-H_2. Therefore, the combination of Y doping and H_2 reduction is responsible for the high degradation rate.

3.3. Mechanism Analysis

RE metal doping can significantly modify the electrical, physical, and chemical properties of TiO_2 photocatalyst and play an effective role for improving photocatalytic performance. Compared to pure TiO_2, 3% Y-doped TiO_2 has a faster degradation rate of RhB, which is attributed to the influence of Y doping. The ionic radius of Y^{3+} (93 pm) is larger than that of Ti^{4+} (68 pm), which is difficult to replace Ti into the TiO_2 lattice directly [25]. Based on the XRD results, no diffraction peak shift is observed for 3% Y-doped TiO_2, demonstrating that Y^{3+} species exists at the crystal boundary or surface rather than in the inner crystalline structure of TiO_2. Furthermore, the survey scanning the XPS spectra (Figure S2) shows that a weak Y 3d peak is observed at ~158 eV, indicating the presence of Y^{3+} species on the surface of 3% Y-TiO_2. Based on XRD and XPS, the Y^{3+} species might be deposited on the surface of TiO_2. Given that the work function (Φ) of RE metals is lower than that of titanium, RE^{3+} has more tendencies to attract the e^- from the sample surface compared with Ti ions, resulting in a reduced e^-–h^+ pair recombination rate. In addition, 3% Y-TiO_2 with a higher specific surface area has more reactive active sites compared with pure TiO_2, which also helps to improve the photocatalytic performance. Moreover, UV–vis DRS revealed that 3% Y-TiO_2 has higher light absorption capacities in their visible region than pure TiO_2, resulting in lower E_g values. However, an excessive amount of metal dopants may lead to a decline in photodegradation efficiency towards pollutants by reducing the yield of photoinduced e^-–h^+ pairs (Figure S1b). Therefore, 3% Y doping is the most suitable doping amount and selected as the subsequent research object in our work.

The reduction treatment of TiO_2 by H_2 is also one of the important methods to improve its photocatalytic performance. Compared to pure TiO_2 and 3% Y-TiO_2, the specific surface areas of TiO_2-H_2 significantly decreased, indicating that the reaction active sites decreased. However, TiO_2-H_2 also had a faster degradation rate of RhB, which is attributed to the changes in microstructure caused by reduction treatment. The remarkable feature of reduced TiO_2 by H_2 is its disordered shell filled with a limited amount of O_Vs or Ti^{3+}, which is consistent with the HRTEM and XPS results. Furthemore, the significant decrease in E_g values of TiO_2-H_2 is due to the significant increase in the sample's absorption capacity for visible light according to UV–vis DRS results. Compared with the RE metal doping, O_V or Ti^{3+} is a kind of self-doping of the crystal itself without introducing any impurity element, which is considered to reflect the influence of the internal modification of TiO_2 on its physicochemical and photocatalytic performance, such as tuning optical absorption, reducing E_g, and increasing carrier concentration [31].

Under the simultaneous action of Y doping and reduction treatment, 3% Y-TiO_2-H_2 exhibited a higher photocatalytic degradation ability than any single-modified catalyst. Thus, a possible photocatalytic mechanism for 3% Y-TiO_2-H_2 nanoparticles is proposed (Figure 7). The disordered shell of reduced 3% Y-TiO_2-H_2 is filled with a limited amount of O_Vs and Ti^{3+}, which significantly reduces the E_g of TiO_2 and remarkably increases the absorption of visible light. The formation of a defective energy level caused by O_V and Ti^{3+} below the conduction band of TiO_2 decreases the excitation energy, resulting in highly active photocatalysts [42]. The incorporation of Y^{3+} on the surface of TiO_2 increases the charge separation by acting as an electron trapper, consequently produces more e^- for reaction on the surface of the catalyst, and reduces the e^--h^+ recombination rate of photocatalyst. In addition to reducing carrier recombination, as a member of RE elements, Y doping broadens the range of light absorption and increases the photoactivity of TiO_2; this phenomenon is consistent with the DRS and photodegradation results. In conclusion, the more reactive active sites, the rapid interfacial charge transfer, and stronger optical absorption of 3% Y-TiO_2-H_2 caused by Y doping should be the reason for the higher rate of photocatalytic reactions than those of undoped TiO_2-H_2 [43]. Their photocatalytic process is such that, under simulated sunlight irradiation, e^- is excited from VB to CB of 3% Y-TiO_2-H_2, and h^+ in VB is abandoned. Generated charge carriers react with oxygen molecules, water molecules, or OH^- to produce oxidative species for the degradation of organic dye in the aqueous solution, such as hydroxyl radicals (•OH) and ($•O_2^-$).

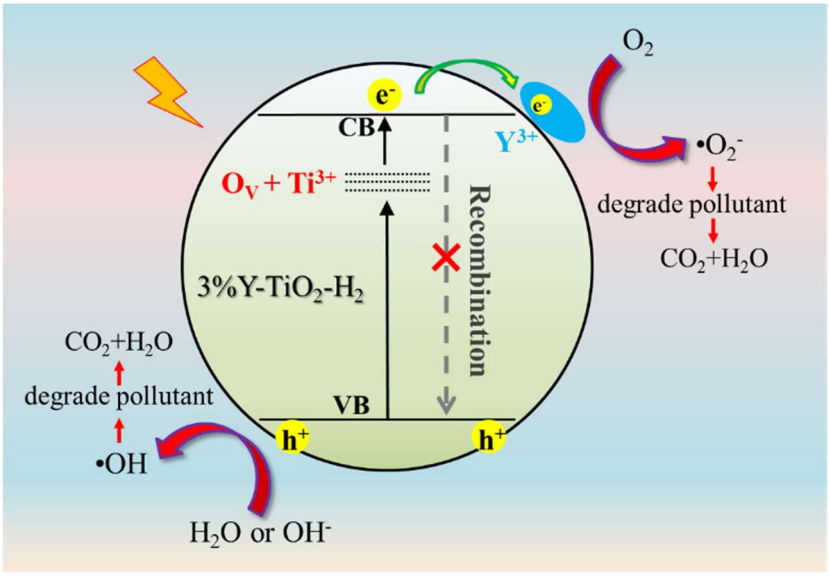

Figure 7. Schematic of the photodegradation of RhB in 3% Y-TiO_2-H_2 nanoparticles.

4. Conclusions

Y doping and the reduction treatment of TiO_2 have been widely proven to be an effective way to improve their photocatalytic performance, respectively. In this work, the coupling treatment of Y doping and reduction of TiO_2 can further improve the photocatalytic performance, which is better than any individual method. In summary, pure TiO_2 and 3% Y-TiO_2 were prepared by a one-step hydrothermal method. Reduced TiO_2-H_2 and 3% Y-TiO_2-H_2 were obtained through the thermal conversion treatment of Ar-H_2 atmosphere at 500 °C for 3 h. All samples show the single anatase phase, and no diffraction peak shift is observed. The photodegradation efficiency of pure TiO_2, 3% Y-TiO_2, TiO_2-H_2, and 3% Y-TiO_2-H_2 on RhB gradually increased. The 3% Y-TiO_2-H_2 exhibits the best photocatalytic performance for the degradation of RhB among these four samples, which can be totally degraded in 20 min. The key factors for the improved photocatalytic performance of 3% Y-TiO_2-H_2 could be attributed to the synergistic effect of Y doping and the reduction of TiO_2. Y metal-ion doping broadened the range of light absorption and reduced the charge recombination rates. Reduction treatment can cause TiO_2 to be enveloped by disordered shells, and O_Vs and Ti^{3+} species efficiently reduced the E_g of TiO_2, remarkably increasing the absorption of light. The synergistic effect of rapid interfacial charge transfer and the stronger optical absorption of 3% Y-TiO_2-H_2 caused by Y doping and reduction treatment should be the reason for the high photocatalytic efficiency. The discovery of this work provides a new perspective for the improvement of other photocatalysts by combining doping and reduction to modify traditional photocatalytic materials and further improve their performance.

Supplementary Materials: The following supporting information can be downloaded at: https://www.mdpi.com/article/10.3390/nano13152266/s1, Figure S1: XRD patterns (a) and degradation curves (b) of pure TiO_2 and various Y-doped TiO_2 (1~5%) samples; Figure S2. Survey scanning XPS spectra of TiO_2, 3% Y-TiO_2, TiO_2-H_2 and 3% Y-TiO_2-H_2 samples. Figure S3. XPS spectra of Ti 2p for TiO_2, 3%Y-TiO_2, TiO_2-H_2 and 3%Y-TiO_2-H_2 samples.

Author Contributions: Conceptualization, X.L. (Xijuan Li) and H.Z.; experiment, X.L. (Xijuan Li) and H.Z., methodology and writing, X.L. (Xijuan Li) and H.Z.; formal analysis, X.L. (Xia Li), H.Z. and Y.W.; investigation, X.L. (Xijuan Li) and H.Z.; writing—original draft preparation, X.L. (Xijuan Li) and H.Z.; writing—review and editing, H.Z., Y.W. and J.L.; review—comment and editing, J.L., K.Y. and J.W.; supervision, H.Z. and K.Z. All authors have read and agreed to the published version of the manuscript.

Funding: This work was supported by the National Natural Science Foundation of China (NSFC No. U1904213 and 52202137), State Key Laboratory of Mechanics and Control of Mechanical Structures (Nanjing University of Aeronautics and Astronautics) (MCMS-E-0521G02), a Project Funded by the Priority Academic Program Development of Jiangsu Higher Education Institutions (PAPD), and Jiangsu Funding Program for Excellent Postdoctoral Talent.

Institutional Review Board Statement: Not applicable.

Informed Consent Statement: Not applicable.

Data Availability Statement: All data generated or analyzed during this work are included in this published article.

Conflicts of Interest: The authors declare no conflict of interest.

References

1. Fujishima, A.; Honda, K. Electrochemical Photolysis of Water at a Semiconductor Electrode. *Nature* **1972**, *238*, 37–38. [CrossRef] [PubMed]
2. Fujishima, A.; Rao, T.N.; Tryk, D.A. Titanium dioxide photocatalysis. *J. Photochem. Photobiol. C Photochem. Rev.* **2000**, *1*, 27–47. [CrossRef]
3. Chen, X.; Mao, S.S. Titanium Dioxide Nanomaterials: Synthesis, Properties, Modifications, and Applications. *Chem. Rev.* **2007**, *107*, 2891–2959. [CrossRef] [PubMed]
4. Guo, Q.; Zhou, C.; Ma, Z.; Yang, X. Fundamentals of TiO_2 Photocatalysis: Concepts, Mechanisms, and Challenges. *Adv. Mater.* **2019**, *31*, 1901997. [CrossRef]
5. Wu, J.; Hao, J.; Guo, W.; Chen, J.; Min, Y. Regulating photocatalysis by the oxidation state of titanium in TiO_2/TiO. *J. Colloid Interface Sci.* **2022**, *613*, 616–624. [CrossRef]
6. Liccardo, L.; Bordin, M.; Sheverdyaeva, P.M.; Belli, M.; Moras, P.; Vomiero, A.; Moretti, E. Surface Defect Engineering in Colored TiO_2 Hollow Spheres Toward Efficient Photocatalysis. *Adv. Funct. Mater.* **2023**, *33*, 2212486. [CrossRef]
7. Noman, M.T.; Ashraf, M.A.; Ali, A. Synthesis and applications of nano-TiO2: A review. *Environ. Sci. Pollut. Res.* **2019**, *26*, 3262–3291. [CrossRef]
8. Schneider, J.; Matsuoka, M.; Takeuchi, M.; Zhang, J.; Horiuchi, Y.; Anpo, M.; Bahnemann, D.W. Understanding TiO_2 Photocatalysis: Mechanisms and Materials. *Chem. Rev.* **2014**, *114*, 9919–9986. [CrossRef]
9. Nakata, K.; Fujishima, A. TiO_2 photocatalysis: Design and applications. *J. Photochem. Photobiol. C Photochem. Rev.* **2012**, *13*, 169–189. [CrossRef]
10. Du, X.; Wu, Y.; Kou, Y.; Mu, J.; Yang, Z.; Hu, X.; Teng, F. Amorphous carbon inhibited TiO_2 phase transition in aqueous solution and its application in photocatalytic degradation of organic dye. *J. Alloys Compd.* **2019**, *810*, 151917. [CrossRef]
11. Bayan, E.M.; Lupeiko, T.G.; Pustovaya, L.E.; Volkova, M.G.; Butova, V.V.; Guda, A.A. Zn–F co-doped TiO_2 nanomaterials: Synthesis, structure and photocatalytic activity. *J. Alloys Compd.* **2020**, *822*, 153662. [CrossRef]
12. Naldoni, A.; Altomare, M.; Zoppellaro, G.; Liu, N.; Kment, S.; Zboril, R.; Schmuki, P. Photocatalysis with Reduced TiO_2: From Black TiO_2 to Cocatalyst-Free Hydrogen Production. *ACS Catal.* **2019**, *9*, 345–364. [CrossRef]
13. Kusiak-Nejman, E.; Morawski, A.W. TiO_2/graphene-based nanocomposites for water treatment: A brief overview of charge carrier transfer, antimicrobial and photocatalytic performance. *Appl. Catal. B Environ.* **2019**, *253*, 179–186. [CrossRef]
14. Obata, K.; Kishishita, K.; Okemoto, A.; Taniya, K.; Ichihashi, Y.; Nishiyama, S. Photocatalytic decomposition of NH3 over TiO2 catalysts doped with Fe. *Appl. Catal. B Environ.* **2014**, *160–161*, 200–203. [CrossRef]
15. Md Saad, S.K.; Ali Umar, A.; Ali Umar, M.I.; Tomitori, M.; Abd Rahman, M.Y.; Mat Salleh, M.; Oyama, M. Two-Dimensional, Hierarchical Ag-Doped TiO_2 Nanocatalysts: Effect of the Metal Oxidation State on the Photocatalytic Properties. *ACS Omega* **2018**, *3*, 2579–2587. [CrossRef]
16. Tbessi, I.; Benito, M.; Molins, E.; Liorca, J.; Touati, A.; Sayadi, S.; Najjar, W. Effect of Ce and Mn co-doping on photocatalytic performance of sol-gel TiO_2. *Solid State Sci.* **2019**, *88*, 20–28. [CrossRef]
17. Asahi, R.; Morikawa, T.; Ohwaki, T.; Aoki, K.; Taga, Y. Visible-Light Photocatalysis in Nitrogen-Doped Titanium Oxides. *Science* **2001**, *293*, 269–271. [CrossRef]
18. Weon, S.; Kim, J.; Choi, W. Dual-components modified TiO_2 with Pt and fluoride as deactivation-resistant photocatalyst for the degradation of volatile organic compound. *Appl. Catal. B Environ.* **2018**, *220*, 1–8. [CrossRef]
19. Al-Azri, Z.H.N.; Chen, W.-T.; Chan, A.; Jovic, V.; Ina, T.; Idriss, H.; Waterhouse, G.I.N. The roles of metal co-catalysts and reaction media in photocatalytic hydrogen production: Performance evaluation of M/TiO_2 photocatalysts (M=Pd, Pt, Au) in different alcohol–water mixtures. *J. Catal.* **2015**, *329*, 355–367. [CrossRef]
20. Ayekoe, P.Y.; Robert, D.; Goné, D.L. Preparation of effective TiO_2/Bi_2O_3 photocatalysts for water treatment. *Environ. Chem. Lett.* **2016**, *14*, 387–393. [CrossRef]
21. Chen, Y.; Huang, W.; He, D.; Situ, Y.; Huang, H. Construction of Heterostructured g-C_3N_4/Ag/TiO_2 Microspheres with Enhanced Photocatalysis Performance under Visible-Light Irradiation. *ACS Appl. Mater. Interfaces* **2014**, *6*, 14405–14414. [CrossRef] [PubMed]

22. Tao, X.; Zhu, L.; Wang, X.; Chen, X.; Liu, X. Preparation of Zr/Y co-doped TiO_2 photocatalyst and degradation performance of hydroquinone. *Environ. Sci. Pollut. Res.* **2022**, *29*, 40854–40864. [CrossRef] [PubMed]
23. Li, J.; Chu, B.; Xie, Z.; Deng, Y.; Zhou, Y.; Dong, L.; Li, B.; Chen, Z. Mechanism and DFT Study of Degradation of Organic Pollutants on Rare Earth Ions Doped TiO_2 Photocatalysts Prepared by Sol-Hydrothermal Synthesis. *Catal. Lett.* **2022**, *152*, 489–502. [CrossRef]
24. Bingham, S.; Daoud, W.A. Recent advances in making nano-sized TiO_2 visible-light active through rare-earth metal doping. *J. Mater. Chem.* **2011**, *21*, 2041–2050. [CrossRef]
25. Reszczyńska, J.; Grzyb, T.; Wei, Z.; Klein, M.; Kowalska, E.; Ohtani, B.; Zaleska-Medynska, A. Photocatalytic activity and luminescence properties of RE^{3+}–TiO_2 nanocrystals prepared by sol–gel and hydrothermal methods. *Appl. Catal. B Environ.* **2016**, *181*, 825–837. [CrossRef]
26. Gao, H.; Liu, J.; Zhang, J.; Zhu, Z.; Zhang, G.; Liu, Q. Influence of carbon and yttrium co-doping on the photocatalytic activity of mixed phase TiO_2. *Chin. J. Catal.* **2017**, *38*, 1688–1696. [CrossRef]
27. Wang, Y.; Lu, K.; Feng, C. Photocatalytic degradation of methyl orange by polyoxometalates supported on yttrium-doped TiO_2. *J. Rare Earths* **2011**, *29*, 866–871. [CrossRef]
28. Wu, Y.; Gong, Y.; Liu, J.; Zhang, Z.; Xu, Y.; Ren, H.; Li, C.; Niu, L. B and Y co-doped TiO_2 photocatalyst with enhanced photodegradation efficiency. *J. Alloys Compd.* **2017**, *695*, 1462–1469. [CrossRef]
29. Tian, X.; Huang, S.; Wang, L.; Li, L.; Lou, Z.; Huang, S.; Zhou, Z. Mitigation of low methane content landfill gas through visible-near-infrared photocatalysis over Y_2O_3:Er^{3+}/Graphene/TiO_2. *Appl. Surf. Sci.* **2018**, *456*, 854–860. [CrossRef]
30. Xing, M.; Zhang, J.; Chen, F.; Tian, B. An economic method to prepare vacuum activated photocatalysts with high photo-activities and photosensitivities. *Chem. Commun.* **2011**, *47*, 4947–4949. [CrossRef]
31. Eom, J.-Y.; Lim, S.-J.; Lee, S.-M.; Ryu, W.-H.; Kwon, H.-S. Black titanium oxide nanoarray electrodes for high rate Li-ion microbatteries. *J. Mater. Chem. A* **2015**, *3*, 11183–11188. [CrossRef]
32. Tian, M.; Mahjouri-Samani, M.; Eres, G.; Sachan, R.; Yoon, M.; Chisholm, M.F.; Wang, K.; Puretzky, A.A.; Rouleau, C.M.; Geohegan, D.B.; et al. Structure and Formation Mechanism of Black TiO_2 Nanoparticles. *ACS Nano* **2015**, *9*, 10482–10488. [CrossRef]
33. Wang, Z.; Yang, C.; Lin, T.; Yin, H.; Chen, P.; Wan, D.; Xu, F.; Huang, F.; Lin, J.; Xie, X.; et al. Visible-light photocatalytic, solar thermal and photoelectrochemical properties of aluminium-reduced black titania. *Energy Environ. Sci.* **2013**, *6*, 3007–3014. [CrossRef]
34. Chen, J.; Ding, Z.; Wang, C.; Hou, H.; Zhang, Y.; Wang, C.; Zou, G.; Ji, X. Black Anatase Titania with Ultrafast Sodium-Storage Performances Stimulated by Oxygen Vacancies. *ACS Appl. Mater. Interfaces* **2016**, *8*, 9142–9151. [CrossRef]
35. Zhu, Q.; Peng, Y.; Lin, L.; Fan, C.-M.; Gao, G.-Q.; Wang, R.-X.; Xu, A.-W. Stable blue TiO_{2-x} nanoparticles for efficient visible light photocatalysts. *J. Mater. Chem. A* **2014**, *2*, 4429–4437. [CrossRef]
36. Zuo, F.; Wang, L.; Wu, T.; Zhang, Z.; Borchardt, D.; Feng, P. Self-Doped Ti3+ Enhanced Photocatalyst for Hydrogen Production under Visible Light. *J. Am. Chem. Soc.* **2010**, *132*, 11856–11857. [CrossRef]
37. Wei, K.; Wang, B.; Hu, J.; Chen, F.; Hao, Q.; He, G.; Wang, Y.; Li, W.; Liu, J.; He, Q. Photocatalytic properties of a new Z-scheme system BaTiO3/In2S3 with a core–shell structure. *RSC Adv.* **2019**, *9*, 11377–11384. [CrossRef]
38. Yan, Y.; Hao, B.; Wang, D.; Chen, G.; Markweg, E.; Albrecht, A.; Schaaf, P. Understanding the fast lithium storage performance of hydrogenated TiO_2 nanoparticles. *J. Mater. Chem. A* **2013**, *1*, 14507–14513. [CrossRef]
39. Awan, I.T.; Lozano, G.; Pereira-da-Silva, M.A.; Romano, R.A.; Rivera, V.A.G.; Ferreira, S.O.; Marega, E. Understanding the electronic properties of $BaTiO_3$ and Er^{3+} doped $BaTiO_3$ films through confocal scanning microscopy and XPS: The role of oxygen vacancies. *Phys. Chem. Chem. Phys.* **2020**, *22*, 15022–15034.
40. Jiang, L.; Huang, Y.; Liu, T. Enhanced visible-light photocatalytic performance of electrospun carbon-doped TiO_2/halloysite nanotube hybrid nanofibers. *J. Colloid Interface Sci.* **2015**, *439*, 62–68. [CrossRef]
41. Shi, L.; Zhou, W.; Li, Z.; Koul, S.; Kushima, A.; Yang, Y. Periodically Ordered Nanoporous Perovskite Photoelectrode for Efficient Photoelectrochemical Water Splitting. *ACS Nano* **2018**, *12*, 6335–6342. [CrossRef] [PubMed]
42. Reszczyńska, J.; Grzyb, T.; Sobczak, J.W.; Lisowski, W.; Gazda, M.; Ohtani, B.; Zaleska, A. Visible light activity of rare earth metal doped (Er^{3+}, Yb^{3+} or Er^{3+}/Yb^{3+}) titania photocatalysts. *Appl. Catal. B Environ.* **2015**, *163*, 40–49. [CrossRef]
43. Reszczyńska, J.; Grzyb, T.; Sobczak, J.W.; Lisowski, W.; Gazda, M.; Ohtani, B.; Zaleska, A. Lanthanide co-doped TiO_2: The effect of metal type and amount on surface properties and photocatalytic activity. *Appl. Surf. Sci.* **2014**, *307*, 333–345. [CrossRef]